J. Cent. South Univ. (2013) 20: 149−155
DOI: 10.1007/s11771-013-1470-6

Springer

Pressure fluctuation and its influencing factors in circulating water pump

DAI Cui(代翠), KONG Fan-yu(孔繁余), DONG Liang(董亮)

Research Center of Fluid Machinery Engineering and Technology, Jiangsu University, Zhenjiang 212013, China

Abstract: In order to investigate the effect of sampling frequency and time on pressure fluctuations, the three-dimensional unsteady numerical simulations were conducted in a circulating water pump. Through comparison of turbulence models with hydraulic performance experiment, SST *k-ω* model was confirmed to study the rational determination of sampling frequency and time better. The Fast Fourier Transform (FFT) technology was then adopted to process those fluctuating pressure signals obtained. On these bases, the characteristics of pressure fluctuations acting on the tongue were discussed. It is found that aliasing errors decrease at higher sampling frequency of 17 640 Hz, but not at a lower sampling frequency of 1 764 Hz. Correspondingly, an output frequency range ten-times wider is obtained at 17 640 Hz. Compared with 8R, when the sampling time is shorter, the amplitudes may be overvalued, and the frequencies and amplitudes of low-frequency fluctuations can not be well predicted. The frequencies at the tongue are in good agreement with the values calculated by formula and the frequency compositions less than the blade passing frequency are accurately predicted.

Key words: circulating water pump; turbulence model; sampling frequency; sampling time; pressure fluctuation

1 Introduction

Pressure fluctuations, which are responsible for unsteady dynamic forces, will give rise to vibration of pump components and generate hydraulic noises. Due to its huge impact on pump design and structural vibrations, the investigation of pressure fluctuations in pumps is of continuous interest. It is principally a consequence of the interaction of nonuniform outflux from impeller to tongue [1–3].

In the past, many numerical and experimental investigations have been carried out to capture the unsteady interaction and unveil the frequency characteristics of pressure fluctuations. In terms of data analysis, the Fast Fourier Transform (FFT) method has been used to obtain the amplitudes of pressure fluctuations as a function of position and flow-rate [4]. PARRONDO-GAYO et al [5] have investigated the unsteady pressure distribution existing in the volute of a conventional centrifugal pump volute, by means of four piezoresistive pressure transducers mounted at 36 locations around the front side of the volute casing. The experiments have demonstrated the strong increase in the magnitude of dynamic forces and dipole-like sound generation in off-design conditions. BARRIO et al [6] have presented a study on the fluid-dynamic fluctuations in a centrifugal pump with different radial gaps between the impeller and the volute. For a given impeller diameter, the dynamic load increases for off-design conditions, especially for the low range of flow rates, whereas the progressive reduction of the impeller-tongue gap brings about corresponding increments in dynamic load. WANG and TSUKAMOTO [7] have conducted a study on the unsteady phenomena under the off-design conditions of a diffuser pump. SOLIS et al [8] have studied numerically the influence of splitter blades and radial gap on the reduction of pressure fluctuation levels at the blade passage frequency in a volute type centrifugal pump, employing Unsteady Reynolds Averaged Navier-Stokes (URANS) approach to solve the unsteady flow, and have pointed out the fact that assuming the flow close to a fully developed condition at outlet provides better results concerning the pressure amplitude levels.

However, in their efforts to illustrate the leading role of the tongue in the impeller-volute interaction, an unanswered question about the validity and usefulness of FFT and its application to frequency amplitude domain analysis are totally neglected. The sampling frequency and time are always determined with a certain randomicity, leading to the final results away from accuracy. MAJIDI [9] has predicted the impeller–volute interaction and obtained the unsteady pressure

Foundation item: Project supported by the Priority Academic Development Program of Jiangsu Higher Education Institutions, China; Project (CXZZ12_0680) supported by Postgraduate Innovation Foundation of Jiangsu Province, China; Project(12JDG082) supported by the Advanced Talent Foundation of Jiangsu University, China
Received date: 2011–11–28; **Accepted date:** 2012–06–30
Corresponding author: DONG Liang, PhD; Tel: +86−13236358677; E-mail: edongliang@yahoo.com

distribution in the impeller and volute casing with a sampling frequency of 4 940 Hz (the time step is 2.024 3×10^{-4} s) and approximately five revolutions (1 000 time steps). In SOLIS's works, the time step for unsteady calculations has been set to be 5.10×10^{-5} s and to have a good frequency resolution concerning the frequency analysis, ten revolutions are conducted.

In this work, the effort to ascertain the principles of sampling frequency and time for a good accuracy of pressure fluctuations was made. The three-dimensional unsteady flow numerical simulation in the suction chamber, circular pumping chamber, impeller, inlet and outlet as the mathematical model was calculated with sliding mesh technology. In addition, in consideration of the flow characteristics of a low Reynolds number in the pump, two turbulence models were compared to discard any impact on the numerical results. In the end, the pressure fluctuation characteristics at the tongue were studied.

2 Numerical simulation

2.1 Pump geometry

The simulated object is a single-stage circulating water pump. Its design parameters are as follows: Q=2 m^3/h, H=2.8 m and n=2 940 r/min. And, the main geometric parameters are illustrated in Table 1. Then, the blade passing frequency can be calculated to be 392 Hz (the rotation frequency of 49 Hz multiplied by the number of blades) as follows [10]:

$$f=nZi/60 \quad (1)$$

where n, Z and i are the rotating speed, the number of blades and harmonic orders, respectively.

Table 1 Main geometric parameters of simulated pump

Parameter	Value
Impeller inlet diameter/mm	30
Impeller outlet diameter/mm	53
Impeller width at outlet/mm	4
Volute base circle diameter/mm	73
Volute width at base circle/mm	14
Blade number	8
Blade outlet angle/(°)	40

2.2 Mesh generation

The numerical simulations of pressure fluctuations were carried out using a commercial CFD code, Fluent. In order to minimize the effects of boundary conditions and ensure numerical stability, appropriate extensions were processed in the inlet and outlet pipes. The whole computational domain was divided into five zones including the inlet pipe, suction chamber, impeller, circular chamber and outlet pipe. Structured hexahedral cells were used to define the inlet and outlet domain, and unstructured tetrahedral cells with strong flexibility were used for other domains (see Fig. 1).

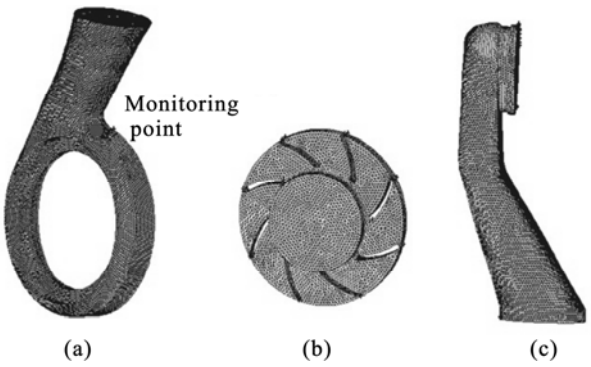

Fig. 1 Sketch of meshes: (a) Circular chamber; (b) Impeller; (c) Suction chamber

The grid quality was checked to ensure the equisize skew and equi-angle skew [11], and they were more than 0.85. In addition, the resulting grid size used during the numerical simulations was determined after a grid independence analysis on the total head, with a simulation carried out in the steady regime. Finally, approximately 1.0×10^6 cells were used for the bulk of numerical simulations, which assured no influence on the numerical results. Rich information of pressure fluctuations was discernible in the virtual sensor placed at tongue in the middle plane. The detailed location of the monitoring point is shown in Fig. 1.

2.3 Numerical methods

In this work, the finite volume method was used for the discretization of governing equations in the space region. The inlet and outlet boundary conditions were set to normal velocity inlet and outflow outlet. The no-slip condition for the boundary layers was imposed over walls and the standard wall function was used. Due to the rotation of impeller, two interfaces between the rotor and stator were formed, one of which was between the suction chamber and the impeller, and the other was between the impeller and the circular chamber. In the steady calculations, based on the Multiple Reference Frame (MRF) model, the inlet pipe, outlet pipe and circular chamber were set in stationary frame, while the impeller was set in rotary frame. The unsteady simulation was initialized from the solution of a steady calculation, whereby it was not performed until the steady convergence was reached. For the unsteady calculation, the Sliding Mesh technique [12] was applied to simulate the rotor−stator interaction. The interfaces between two stationary components, rotary and stationary components, were set to general grid interface and rotor/stator interface, respectively. As for the

discretization in the time domain, the second-order implicit format was adopted. The pressure–velocity coupling was performed using the SIMPLEC algorithm. Second-order format was used for pressure item, and QUICK format for other items. The criterion for convergence was considered to be 10^{-4}, allowing an optimal number of iterations for each time step.

3 Turbulence models

The Reynolds number in the simulated pump can be calculated to be 2.156×10^5 as follows [13]:

$$Re=\frac{u_2D_2/2}{\nu} \tag{2}$$

where u_2 is the circumferential velocity of impeller outlet, and ν is the kinematic viscosity of transmission medium. LUO et al [13] simulated two semi-open centrifugal impellers, whose diameter were 36 mm and Reynolds number equaled 3.72×10^5, finding that SST k-ω turbulence model can be used to predict performance with some accuracy. It was also confirmed in the published work of LIU et al [14].

3.1 RNG k-ε turbulence model

The RNG k-ε model, a mathematical technique that can be used to derive a turbulence model similar to the k-ε, results in a modified form of the epsilon equation which attempts to account for the different scales of motion through changes to the production term [15]. In the standard k-ε model, the eddy viscosity is determined from a single turbulence length scale, so the calculated turbulent diffusion occurs only at the specified scale, whereas in reality all scales of motion will contribute to the turbulent diffusion. The transport equations for k and ε are as follows:

$$\frac{\partial(\rho k)}{\partial t}+\frac{\partial(\rho k u_i)}{\partial x_i}=\frac{\partial}{\partial x_j}[\alpha_k\mu_{\text{eff}}\frac{\partial k}{\partial x_j}]+G_k-\rho\varepsilon \tag{3}$$

$$\frac{\partial(\rho\varepsilon)}{\partial t}+\frac{\partial(\rho\varepsilon u_i)}{\partial x_i}=\frac{\partial}{\partial x_j}[\alpha_\varepsilon\mu_{\text{eff}}\frac{\partial\varepsilon}{\partial x_j}]+C_{1\varepsilon}^*\frac{\varepsilon}{k}G_k-C_{2\varepsilon}\frac{\rho\varepsilon^2}{k} \tag{4}$$

where $\mu_{\text{eff}}=\mu+\mu_T$, $\mu_T=\rho C_\mu\dfrac{k^2}{\varepsilon}$, $C_{1\varepsilon}^*=C_{1\varepsilon}-\dfrac{\eta(1-\eta/\eta_0)}{1+\beta\eta^3}$, $\eta=(2E_{ij}\cdot E_{ij})^{1/2}\dfrac{k}{\varepsilon}$, $E_{ij}=\dfrac{1}{2}(\dfrac{\partial u_i}{\partial x_j}+\dfrac{\partial u_j}{\partial x_i})$, $\eta_0=4.377$, $\beta=0.012$, $C_{1\varepsilon}$=1.42, $C_{2\varepsilon}$=1.68, C_μ=0.008 45, $\alpha_k=\alpha_\varepsilon$=1.39.

3.2 SST k-ω turbulence model

The use of a k-ω formulation in the inner parts of the boundary layer makes the SST k-ω turbulence model directly usable all the way down to the wall through the viscous sub-layer, hence the SST k-ω model can be used as a low-Re turbulence model without any extra damping functions [16]. The SST formulation also switches to k-ε behavior in the free-stream and thereby avoids the common k-ω problem that the model is too sensitive to the inlet free-stream turbulence properties. The SST k-ω model does produce a bit too large turbulence levels in regions with large normal strain, like stagnation regions and regions with strong acceleration, but this tendency is much less pronounced than that with a normal k-ε model. The transport equations for k and ω are as follows:

$$\frac{\partial(\rho k)}{\partial t}+\frac{\partial(\rho U_j k)}{\partial x_j}=P_k-\beta'\rho k\omega+\frac{\partial}{\partial x_j}\left[\left(\mu+\frac{\mu_t}{\sigma_{k3}}\right)\frac{\partial k}{\partial x_j}\right] \tag{5}$$

$$\frac{\partial(\rho U_j\omega)}{\partial x_j}=\alpha_3\frac{\omega}{k}P_k-\beta_3\rho k\omega^2+\frac{\partial}{\partial x_j}\left[\left(\mu+\frac{\mu_t}{\sigma_{\omega3}}\right)\frac{\partial\omega}{\partial x_j}\right]+(1-F_1)2\rho\sigma_{\omega2}\frac{1}{\omega}\frac{\partial k}{\partial x_j}\frac{\partial\omega}{\partial x_j} \tag{6}$$

where $F_1=\tanh\left(\arg_1^4\right)$, $F_2=\tanh\left(\arg_2^2\right)$,

$$CD_\omega=\max\left(2\rho\sigma\omega^2\frac{1}{\omega}\frac{\partial k}{\partial x_j}\frac{\partial\omega}{\partial x_j},1.0\times10^{-10}\right),$$

$$\nu_t=\frac{\alpha_1 k}{\max(\alpha_1\omega,SF_2)},$$

$$\arg_1=\min\left[\max\left(\frac{\sqrt{k}}{\beta'\omega y},\frac{500\nu}{y^2\omega}\right),\frac{4\rho\sigma_{\omega2}k}{CD_{kw}y^2}\right],$$

$$\arg_2=\max\left(\frac{2\sqrt{k}}{\beta'\omega y},\frac{500\nu}{y^2\omega}\right),$$

$\phi_3=F_1\phi_1+(1-F_1)\phi_2$, $\beta'=0.09$, $\alpha_1=5/9$, $\beta_1=3/40$, $\sigma_{k1}=2$, $\sigma_{\omega1}=2$, $\alpha_2=0.44$, $\beta_2=0.082\ 8$, $\sigma_{k2}=1$, and $\sigma_{\omega2}=0.856$.

The unsteady flow was simulated using RNG k-ε model and SST k-ω model. In order to verify the accuracy of numerical results, according to GB/T 3216—2005 “Rotadynamic pumps-Hydraulic performance acceptance tests—Grade 1 and 2” [17], the hydraulic performance experiment was conducted on the two level test-bed. The comparison of the experimental results and time-averaged numerical results was made, as shown in Fig. 2.

We can see that the predicted values are more accurate by SST k-ω turbulence model. By it, the total head predicted is less than the experimental value under low flow rate, while more under the design and high flow rate. The errors of the total head and efficiency are

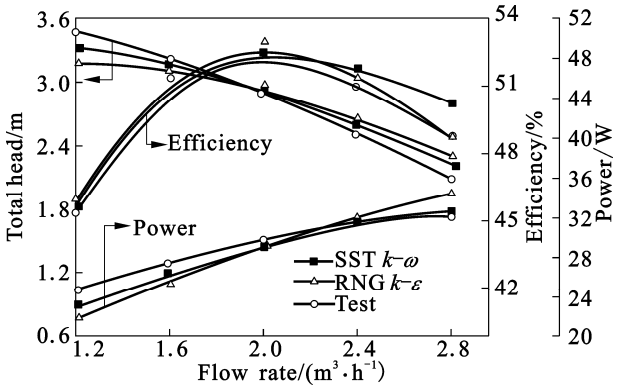

Fig. 2 Comparison of performance curves

within 5% (apart from $0.6Q_d$ and $1.4Q_d$). From this, we can conclude that the internal unsteady flow obtained by SST k-ω model is more credible, and it can be used to analyze the internal pressure fluctuations induced by unsteady flow.

4 Effect of sampling frequency and time

After numerical simulation, the pressure fluctuations over a certain period of time at different monitoring points were got. Then, FFT was used to decompose a sequence of values into components of different frequencies. Generally, the operation collected signals of pressure fluctuations at a presetting rate and a fixed resolution. In the research of the effects of sampling frequency and time on pressure fluctuations, six schemes were designed (see Table 2). Let R denote the time that the pump makes one revolution. To achieve the convergence of unsteady calculations, approximately ten revolutions were necessary to obtain a periodic unsteady solution of the static pressure. Then, additional revolutions ($2R$, $4R$ and $8R$) with respect to different sampling frequencies were processed at the tongue under $1.2Q_d$. The frequency spectra of pressure fluctuations after FFT for different sampling time at a sampling frequency of 17 640 Hz are shown in Fig. 3. Similarly, the situations of pressure fluctuations at 1 764 Hz are shown in Fig. 4. In addition, we studied the pressure fluctuations at 17 640 Hz with frequency ranging from zero to 900 Hz in Fig. 5. The pressure coefficient C_p in y-coordinate is defined as follows [18]:

$$C_p=\Delta p/(0.5\rho u_2^2) \quad (7)$$

where Δp and ρ are the differences between static pressure and the average value, and the water density, respectively.

As it is demonstrated in Fig. 3 and Fig. 4, when the sampling time is same (for example Scheme 1 and Scheme 4), the highest frequency output at a sampling

Table 2 Numeric schemes

Scheme No.	Sampling frequency/Hz	Sampling time
1	17 640	$2R$
2	17 640	$4R$
3	17 640	$8R$
4	1 764	$2R$
5	1 764	$4R$
6	1 764	$8R$

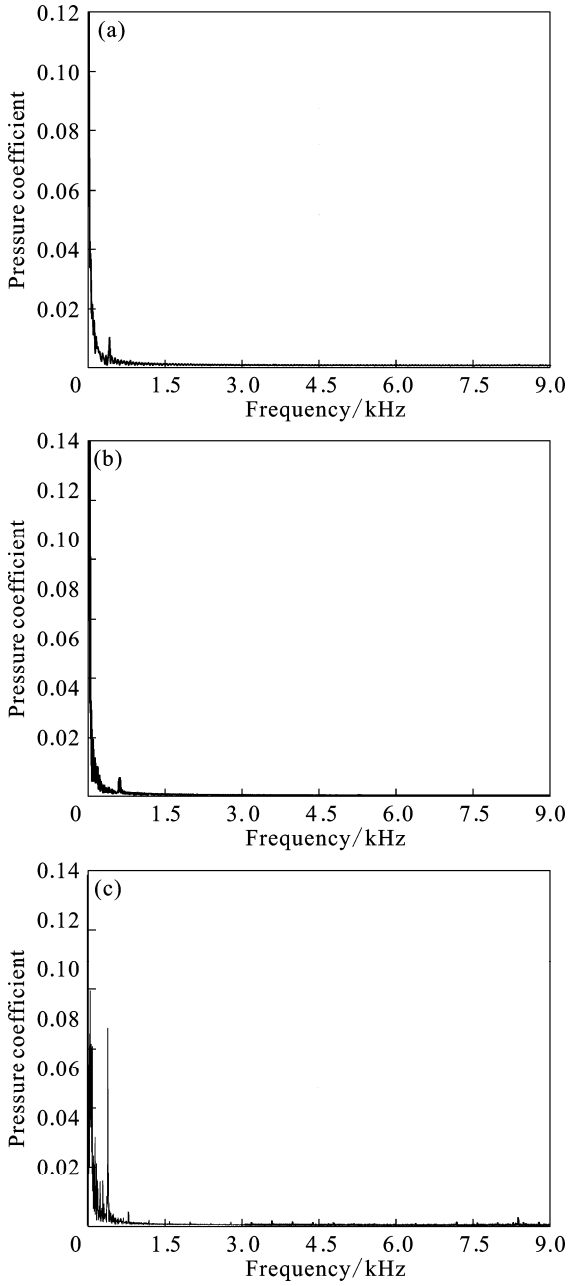

Fig. 3 Frequency spectra of pressure fluctuations at 17 640 Hz: (a) Scheme 1; (b) Scheme 2; (c) Scheme 3

rate of 17 640 Hz is 9 000 Hz, which is ten times that at 1 764 Hz. During FFT, if the sampling frequency is not too high, when higher frequency signals appear, part of

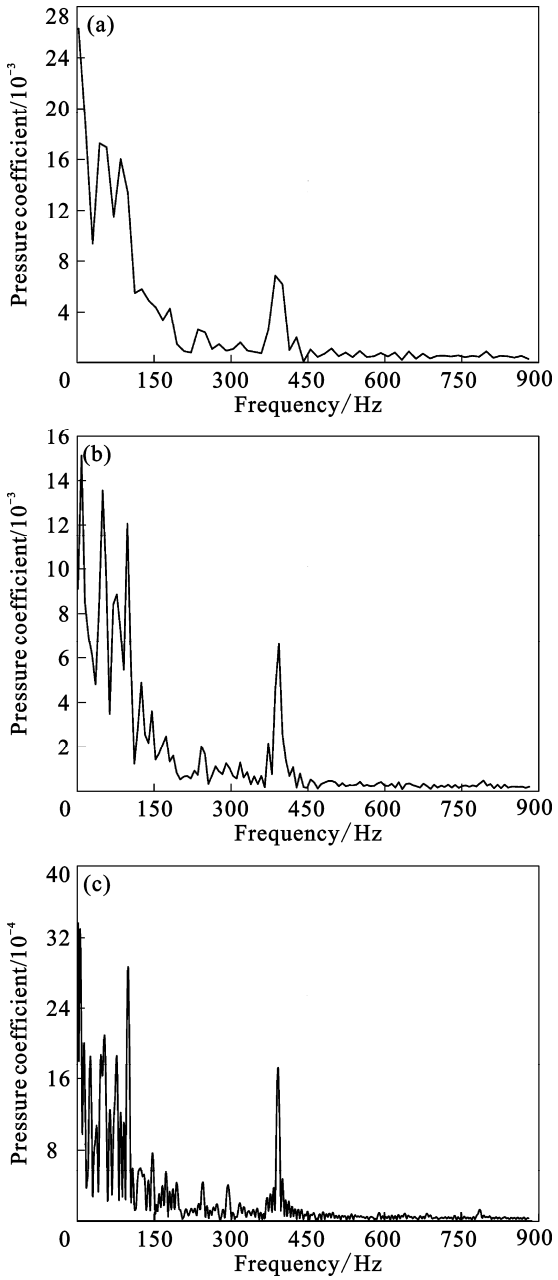

Fig. 4 Frequency spectra of pressure fluctuations at 1 764 Hz: (a) Scheme 4; (b) Scheme 5; (c) Scheme 6

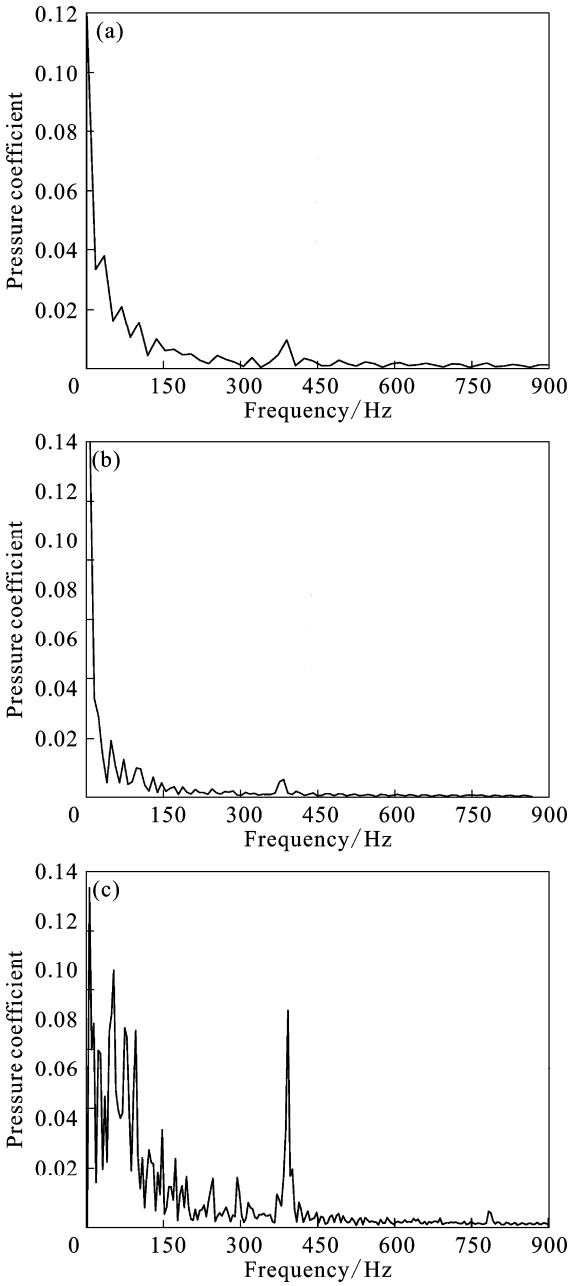

Fig. 5 Frequency spectra of pressure fluctuations at 17 640 Hz with frequency ranging from zero to 900 Hz: (a) Scheme 1; (b) Scheme 2; (c) Scheme 3

the signals will fold back or confuse into the frequency, causing aliasing errors. This is demonstrated by comparing the pressure fluctuations in Scheme 4 in Fig. 4 and Scheme 1 in Fig. 5 under the same sampling time. To avoid aliasing, the sampling frequency must be greater than twice the maximum frequency component of the signal to be acquired, according to the principle of Shannon sampling theorem [19]. However, high sampling frequency will make all accidental noise collected, interfering with the true signals. The previous studies show that the frequencies of pressure fluctuations in centrifugal pumps cover a wider range, and its change is complex. So, to adequately preserve the shape of signals, we suggest that the sampling frequency is set to be 17 640 Hz. Correspondingly, the time step for the unsteady calculation is set to be 5.669×10^{-5} s.

By comparing the frequency spectra of pressure fluctuations in Fig. 4 and Fig. 5, we can find under the same sampling frequency, when the sampling time is shorter, the amplitudes may be overvalued, and the frequencies and amplitudes of low-frequency fluctuations cannot be well predicted. Due to a certain frequency resolution in FFT results, only a limited spectrum values can be got. So, the values in the interval will leak into the surrounding discrete frequencies,

causing truncation errors. To reduce truncation errors, we should try to increase the sampling time, or fill zero in the end of data. Although the latter can encrypt spectrum lines in FFT analysis and improve the frequency resolution, too much zeros in the end will cause waveform distortion in frequency domain. By increasing the sampling time, the frequency resolution can be improved and the composition of pressure fluctuations can be accurately analyzed. But, it will greatly consume more time. The 8*R* is suggested by which the time is consumed and the calculated results are acceptable in the engineering.

5 Pressure fluctuations at tongue

Much data of pressure fluctuations at the tongue under different conditions were obtained at the recommended sampling frequency and time in Fig. 6. The relative frequency in *x*-coordinate was defined as the ratio of the actual frequency to 48.8 Hz.

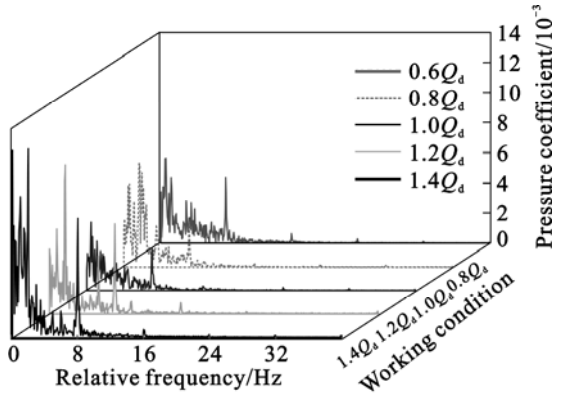

Fig. 6 Frequency spectra of pressure fluctuations at tongue under different conditions

It is observed that there exits pressure fluctuations at 48.8 Hz, 391.9 Hz and their harmonics, which are in agreement with the rotation frequency (49 Hz) and the blade passing frequency (392 Hz), indicating the interaction between impeller and tongue and the effect of the number of blades. Also, we can find that the fluctuations less than the blade passing frequency dominate under each condition, and their corresponding peak values are obvious. Close to design condition, the amplitude decreases, and it will increase when the flow rate changes.

6 Conclusions

1) SST *k*-*ω* model is in good agreement with the hydraulic performance experiment, and is confirmed to be better than RNG *k*-*ε* turbulence model. The internal unsteady flow obtained by SST *k*-*ω* model is more credible, and can be adopted to predict the internal pressure fluctuations.

2) Higher sampling frequency (17 640 Hz) decreases aliasing errors, with a ten times of frequency range respecting to a lower sampling frequency of 1 764 Hz. The higher the sampling time is, the higher the frequency resolution is. To match the accuracy and time, 5.669×10^{-5} s (the time rotating one degree) and 8 revolutions are suggested.

3) The pressure fluctuations at 48.8 Hz, 391.9 Hz are almost identical to 49 Hz and 392 Hz calculated by the formula. The peak values of the frequencies lower than the blade passing frequency are obvious, indicating their leading role in the pressure fluctuations at the tongue.

References

[1] DONG R, CHU S, KATZ J. Effect of modification to tongue and impeller geometry on unsteady flow, pressure fluctuations, and noise in a centrifugal pump [J]. Journal of Turbomachinery, 1997, 119(3): 506–515.

[2] CHOI J S, McLAUGHLIN D K, THOMPSON D E. Experiments on the unsteady flow field and noise generation in a centrifugal pump impeller [J]. Journal of Sound and Vibration, 2003, 263(3): 493–514.

[3] SPENCE R, AMARAL-TEIXEIRA J. Investigation into pressure pulsations in a centrifugal pump using numerical methods supported by industrial tests [J]. Computers and Fluids, 2008, 37(6): 690–704.

[4] LEE Sang-hyuk, WANG Yi-qi, SONG Jung-il. Fourier and wavelet transformations application to fault detection of induction motor with stator current [J]. Journal of Central South University of Technology, 2010, 17 (1): 93−101.

[5] PARRONDO-GAYO J, GONZÁLEZ-PÉREZ J, FERNÁNDEZ-FRAN COS J. The effect of the operating point on the pressure fluctuations at the blade passage frequency in the volute of a centrifugal pump [J]. Journal of Fluids Engineering, 2002, 124(3): 784–790.

[6] BARRIO R, PARRONDO J, BLANCO E. Numerical analysis of the unsteady flow in the near-tongue region in a volute-type centrifugal pump for different operating points [J]. Computers & Fluids, 2010, 39(5): 859-870.

[7] WANG H, TSUKAMOTO H. Experimental and numerical study of unsteady flow in a diffuser pump at off-design conditions [J]. Journal of Fluids Engineering, 2003, 125(5): 767–778.

[8] SOLIS M, BAKIR F, KHELLADI S. Pressure fluctuations reduction in centrifugal pumps: Influence of impeller geometry and radial gap [C]// ASME 2009 Fluids Engineering Division Summer Meeting. Vail, 2009: 253–265.

[9] MAJIDI K. Numerical study of unsteady flow in a centrifugal pump [J]. Journal of Turbomachinery, 2005, 127(2): 363–371.

[10] DAI Cui. Study on pressure fluctuation of miniature circulation pump [D]. Zhenjiang: Research Center of Fluid Machinery Engineering and Technology, Jiangsu University, 2009: 28. (in

Chinese)

[11] DONG Liang, LIU Hou-lin, TAN Ming-gao, LU Ming-zhen, WANG Yong, WANG Kai. Quality measurement criteria and optimization algorithm of tetrahedral mesh for centrifugal pumps [J]. Journal of Xi'an Jiao Tong University, 2011, 45(11):100–105. (in Chinese)

[12] VASUDEVA-KARANTH K, YAGNESH-SHARMA N. Numerical analysis on the effect of varying number of diffuser vanes on impeller-diffuser flow interaction in a centrifugal fan [J]. World Journal of Modeling and Simulation, 2009, 5(1): 63–71.

[13] LUO Xian-wu, XU Hong-yuan, LIU Shu-hong. Effect of blade lean on mini pump hydraulic performance [J]. Journal of Tsinghua University: Science and Technology, 2005, 45(5): 704–707. (in Chinese)

[14] LIU S H, NISHI M, YOSHIDA K. Impeller geometry suitable for mini turbo-pump [J]. Journal of Fluids Engineering, 2001, 123(3): 500–506.

[15] YAKHOT V, ORSZAG S A, THANGAM S, GATSKI T B, SPEZIALE C G. Development of turbulence models for shear flows by a double expansion technique [J]. Physics of Fluids A, 1992, 4(7): 1510–1520.

[16] MENTER F R. Two-equation eddy-viscosity turbulence models for engineering applications [J]. AIAA Journal, 1994, 32(8): 1598–1605.

[17] GB/T 3216—2005. Rotadynamic pumps-Hydraulic performance acceptance tests–Grade 1 and 2 [S]. Beijing: Standards Press of China, 2006. (in Chinese)

[18] WANG Yang, DAI Cui. Analysis on pressure fluctuation of unsteady flow in a centrifugal pump [J]. Transactions of the Chinese Society for Agricultural Machinery, 2010, 41(3): 91–95. (in Chinese)

[19] FANG Gen-sun. Whittaker–Kotelnikov–Shannon sampling theorem and aliasing error [J]. Journal of Approximation Theory, 1996, 85(2): 115–131.

(Edited by YANG Bing)